Hindawi
Advances in Materials Science and Engineering
Volume 2022, Article ID 9895908, 10 pages
https://doi.org/10.1155/2022/9895908

Research Article

Multiobjective Optimization System of Extrusion Process Parameters for Targeted Microtubes Based on RSM and NSGA-II

Qingqing Zhang, Guobao Jin, and Guanghui Dai

College of Mechanical Engineering, Chaohu University, Hefei 238000, China

Correspondence should be addressed to Qingqing Zhang; lizqq1314@126.com

Received 11 September 2022; Revised 7 October 2022; Accepted 21 October 2022; Published 3 November 2022

Academic Editor: Ghulam Rasool

Copyright © 2022 Qingqing Zhang et al. This is an open access article distributed under the Creative Commons Attribution License, which permits unrestricted use, distribution, and reproduction in any medium, provided the original work is properly cited.

An optimization system of extrusion process parameters was designed to rapidly extrude a microtube with a target diameter and wall thickness for forming medical balloons with personalized size characteristics. Firstly, the double convected pom-pom (DCPP) model was selected for the numerical simulation of the tube extrusion process, and different parameter combinations and their corresponding simulation results were extracted based on orthogonal experiments. Secondly, the nonlinear functional relationships between microtube diameter and wall thickness with extrusion parameters were established based on the response surface model (RSM). Finally, the nondominated sorting genetic algorithm II (NSGA-II) and response surface model (RSM) were mixed to find the optimal parameters of the tube extrusion. The extrusion experiment results, taking three microtubes with different target size characteristics (1, 0.15), (1, 0.2), and (1.5, 0.2) as examples, show that the average error between the actual and predicted values of diameter and wall thickness of three microtubes is 6.53%, where the average diameter error is 7.3%, the wall thickness error is 5.77%, the maximum value is 9%, and the minimum value is only 1.3%.

1. Introduction

Polymer microtubes are used more and more widely in the fields of medicine and optical fiber communication, making polymer microextrusion technology an attractive choice in the manufacture of composite microtubes [1]. However, the difficulty of microtube forming gradually increases due to the gradual reduction of microtubule size and the improvement of geometric accuracy requirements. Examples include tubes for personalized medical balloons since the detailed control of the wall thickness at each end of the balloon depends on the diameter and thickness of the microtubule [2]. It is generally believed that extrusion deformation of the microtube depends on the flow history in extrusion, and the main aspect that should be considered when studying the cross-sectional geometrical characteristics of the tube is the influence of process parameters. Therefore, it is the primary challenge to obtain appropriate extrusion process parameters for precision and rapid manufacturing of steel tubes [3].

Researchers have paid great attention to the influence of extrusion process parameters on the cross-sectional geometrical characteristics (diameter and thickness) of microtubes. Zou [4] and Huang [5] researched the influence of four extrusion process parameters, including dying temperature, screw speed, traction rate, and gas injection flow rate, on the cross-sectional shape accuracy of interventional medical tubes based on an orthogonal test and obtained an optimal parameter set. Henry [6] established the relationship between stretch ratio, solution temperature, polymer molecular weight, and other parameters with the shrinkage of a sleeve and researched the reasonable range of the corresponding parameters. Chen [7] studied the deformation rule of polymer melt after leaving the die and analyzed the influence of the four extrusion process parameters (gas injection pressure, screw speed, traction speed, and die temperature) on the diameter and wall thickness. Gong [8] investigated the effects of microextrusion process parameters on the diameter and wall thickness of the tube using numerical simulation and experimental methods, taking PA11 as the experimental

material. Fu et al. [9] analyzed the effect of different die temperatures on extruding small-bore tubes at the same extrusion speed and analyzed the effect of temperature on the change of the tube dimensions at different extrusion speeds. Jin [10] found that when the screw speed of the extruder increases, the pressure value of the polymer melt in the die flow channel also increases, making the diameter of the extrusion duct increase. It can be seen from the above research studies that the extrusion process parameters have significant influences on the size characteristics of the microtube cross section, and the desired results can be obtained by a large number of extrusion experiments, but it will take a lot of time and consume a lot of experimental materials. In recent years, the efficiency of microtubule forming process parameter design has been continuously improved with the improvement of computing power and the gradual application of numerical simulation methods in extrusion expansion simulation [11–14]. However, the nonlinear relationship between extrusion process parameters and tube size characteristics is rarely reported, especially in the optimization of the extrusion process for multiobjective characteristics. Therefore, it is a very challenging task to establish a multiobjective optimization function with the microtube geometry as the optimization objective and the process parameters as the design variables for quickly obtaining appropriate extrusion process parameters. To address this issue, a multiobjective optimization system of the extrusion process parameters for forming target microtubes was designed in this paper, and the optimization flowchart is shown in Figure 1.

2. Numerical Simulation

2.1. Governing Equation. The polymer melt can be regarded as a continuous medium in the microextrusion process, and its flow state satisfies three basic equations: mass conservation equation (the continuity equation), momentum conservation equation (motion equation), and energy conservation equation (energy equation). The melt flow in the mold passage is assumed to be a steady flow, and the influence of the melt inertia force and gravity can be ignored considering the continuity, stability, and isotherm of the polymer during microextrusion. There is no heat exchange between the melt and the die, and the polymer melt is incompressible. The continuity equation and motion equation at higher extrusion temperatures are described as follows.

The continuity equation is as follows:

$$\nabla \cdot u = 0. \tag{1}$$

The motion equation is as follows:

$$-\nabla p + \nabla \cdot T = 0, \tag{2}$$

where ∇ is the Hamilton differential operator, u is the velocity vector, p is the hydrostatic pressure, and T is the extra stress tensor. It should be noted that the temperature inside the melt is equal everywhere and the temperature gradient is zero when the polymer melt flows isothermally. Therefore, the energy is unchanged and does not need to be solved during the extrusion process.

2.2. Constitutive Equation. The multimode DCPP constitutive equation is used to describe the realistic viscoelastic property of the polymer melt and to relate the dynamics to the kinematics of the above equations in the paper. The model has undergone changes and improvements to make it suitable for software implementation and to introduce a nonzero second normal-stress difference, and the model can be described as the following equation [15, 16]:

$$T_i = \frac{G_i}{1-\xi_i}\left(3\Lambda_i^2 S_i - I\right), \tag{3}$$

where T_i is the viscoelastic extra stress tensor, I is the unit tensor, S_i is the orientation tensor, and Λ_i is the stretching variable, and these are used to describe the behavior of the pom-pom macromolecular. Superscript i denotes the ith relaxation mode. G_i and ξ_i are the shear relaxation modulus and the parameter controlling the second normal-stress difference, respectively. S_i obey (4) and Λ_i obey (5).

$$\lambda_i\left[\left(1-\frac{\xi_i}{2}\right)\overset{\nabla}{S}_i + \frac{\xi_i}{2}\overset{\Delta}{S}_i\right] + \lambda_i(1-\xi_i)[2D:S_i]S_i + \frac{1}{\Lambda_i^2}\left[S_i - \frac{I}{3}\right] = 0, \tag{4}$$

$$\tau_i\frac{D\Lambda_i}{Dt} - \tau_i(2D:S_i)\Lambda_i + (\Lambda_i - 1)e^{2(\Lambda_i - 1)/q_i} = 0, \tag{5}$$

where D is the rate of deformation tensor represented by $D = (\nabla u + \nabla u')/2$, in which u' denotes the transpose of tensor, and superscripts ∇ and Δ denote the upper- and lower-convected derivatives, respectively. λ_i and τ_i are the orientation relaxation time and the stretching relaxation time, and q_i represents the number of branches attached at each extremity of the pom-pom macromolecular.

2.3. Extrusion Die Structure. The straight-through extrusion die was selected and designed in this paper to simulate and experimentally verify the microtube extrusion process of a medical balloon. The schematic diagram of the flow path inside the die is shown in Figure 2. Its main structural parameters are the mandrel outer diameter d_0, the shaping section length L, the die inner diameter D_0, the compression angle a, and the compression ratio e. According to the previous die design research results, the value of each structural parameter is shown in Table 1.

2.4. Material Characterization. The material researched is one kind of polypropylene resin (PP, grade T30S, China National Petroleum Corporation), whose density is 0.91 g/cm^3 under ambient pressure and temperature, the melting temperature is 170°C, and the applicable extrusion temperature ranges from 185 to 275°C. The rheological behavior of the material was tested experimentally at a melt temperature of 200°C with a double barrel capillary rheometer (Rosad-RH7, Malvern, UK). The material parameters of the constitutive equation employed were obtained by fitting the

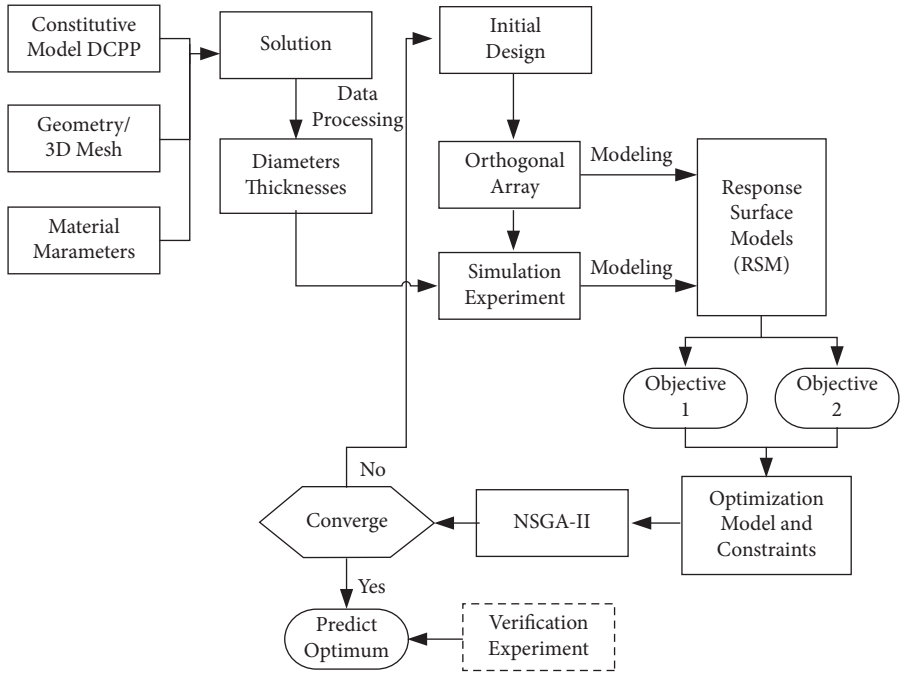

Figure 1: The optimization flowchart of the extrusion process parameter optimization system.

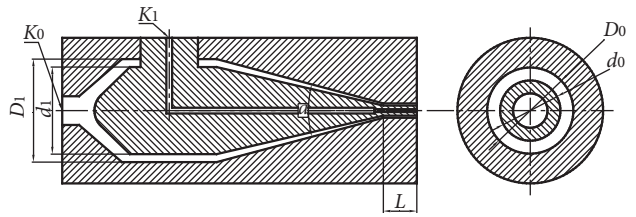

Figure 2: Schematic diagram of microtube mold flow channel.

Table 1: Flow channel structure parameter of microtube extrusion die.

Structural parameters	Value
Mandrel outer diameter d_0	0.7 mm
Shaping section length L	2.3 mm
Die inner diameter D_0	1 mm
Compression angle a	36°
Compression ratio e	588

experimental data as illustrated to endow the model with realistic rheological properties. The model parameters obtained by Tian et al. [16] using the same polymer are adopted.

2.5. Boundary Conditions. The governing equations and extruding processes are solved numerically by the finite element method (FEM). The 3D mesh model of the compression section and shaping section in the microextrusion die was developed with ANSYS GAMBIT. A quarter of the model was selected for calculating the flow channel to reduce the calculation amount and increase the calculation speed since it is an axisymmetric structure. The unstructured hexahedral element is used for discretizing the domain into finite elements, as shown in Figure 3. A refiner mesh generation was adopted near the die exit where the boundary condition suddenly changes from nonslip to free surface, and the meshes were characterized by 10, 120 finite elements.

It is assumed that the upstream flow channel is reasonable to achieve flow balance at the die inlet according to the extrusion process; therefore, a fully expanded axial velocity profile with the volume flow rate Q and the radial velocity being zero ($\mathrm{un} = f(Q)$; $ut = 0$) is applied. The wall slip may have a significant effect on the extrusion flow in some cases, so it has been considered in the mathematical modeling of extrusion flow in previous studies [17], and the Naiver slip boundary condition has been selected [18]. Usual symmetry conditions were set on the symmetry plane. The melt undergoes a free surface flow on the outside of the die. The gas injection condition was the air pressure boundary while the normal force was applied, which was also applied on the free surface. The traction rate was applied at the exit boundary, and stress-free conditions were assumed where the volumetric flow rate Q can be described as the following equation:

$$Q = \left(\frac{R'T}{P+N} + \omega \right) \cdot Q_m, \tag{6}$$

where Q_m is the melt mass flow rate (g/s), P is the pressure before the entrance of the die (N/cm^2), N is the internal pressure (N/cm^2), ω is the specific volume at absolute temperature zero (cm^3/g), R' is the corrected gas constant ($N \cdot cm^3/(cm^2 \cdot g \cdot k)$), and T is the absolute temperature (K).

During the numerical simulation, the finite element algorithm involves a combination of the streamline winding method (SU) and the discrete elastic viscous stress splitting (DEVSS) [19] to obtain a stable solution for the 3D

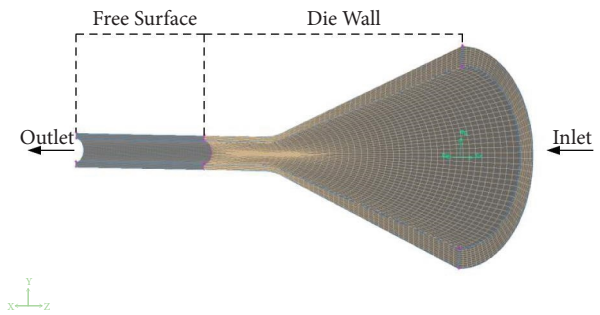

Figure 3: Finite element meshes used in the computation.

viscoelastic squeeze flow. The low interpolations of quadratic velocity and linear pressure functions are employed to reduce the computational cost, and a remeshing technique is employed to obtain the free surface locations.

3. Orthogonal Test and Results

3.1. Orthogonal Test Factor. Compared with multichamber microtubes, single-cavity microtubes are smaller in dimension and simpler in structure. Therefore, it is easier to analyze the influence of the extrusion process on the microtube structure dimension. The simulation process parameters, as well as experimental process parameters of the microtube extrusion, mainly include wall slip, screw speed (volume flow), gas injection volume (gas injection pressure), die temperature, and traction speed [10]. Once the material is determined, the wall slip is also determined because the wall slip is related to the material properties [20]. According to research results, the diameter and wall thickness of the microtubes barely changed at different mold temperatures, and the proper mold temperature can make the polymer melt have proper fluidity [21]. So, the mold temperature was set to 200°C. To sum up, the process parameters selected in this experiment are air injection volume (q ml/min), traction speed (v m/min), and screw speed (n r/min). The process parameter range of the single-cavity microtube extrusion molding experiment was selected according to the preliminary extrusion experiment and material behavior, as shown in Table 2.

3.2. Orthogonal Test Schemes and Results. It is known from Table 2 that there are 3 factors and 4 levels. The $L_4{}^4$ (16) type orthogonal table could be selected for the test [22]. The numerical simulation experiments were conducted with Ansys Polyflow. In this paper, the simulation experiments were performed according to the parameter combinations of the orthogonal table, and the diameters and wall thickness of single-cavity microtubes were researched. Different parameter combinations and their corresponding simulation results according to the orthogonal table are shown in Table 3.

Table 2: Level table of orthogonal test factors.

Levels	Factors		
	A q (ml/min)	B v (m/min)	C n (r/min)
1	3	6	4
2	4	12	8
3	5	18	12
4	6	24	16

4. Model Based on Response Surface Methodology

4.1. Response Surface Methodology (RSM). The nonlinear objective functions were established with the RSM to map the relationships between main process parameters and two-size goals. There are three strategy variables: air injection volume, traction speed, and screw speed, and two goal variables of diameters and wall thicknesses in the model. The RSM models were established for each target variable, respectively. The second-order polynomial function can better represent the relationship between process conditions and assessment indicators than a first-order function, and the amount of fitting calculation required for the second-order polynomial function is less than that of the third-order and higher-order polynomial functions, according to the researchers [23]. The objective function can be defined as follows.

According to the research [24], the second-order polynomial function can better represent the relationship between process conditions and assessment indicators than a first-order function, and the amount of fitting calculation required for the second-order polynomial function is less than that of the third-order and higher-order polynomial functions. Therefore, the second-order polynomial function was selected to establish the nonlinear relationship between the main parameters and the target. The objective function can be defined as follows:

$$f(x) = \beta_0 + \sum_{i=1}^{k} \beta_i X_i + \sum_{i=1}^{k} \beta_{ii} X_i^2 + \sum \sum_{i<j} \beta_{ij} X_i X_j, \quad (7)$$

where k is number of factors, β_0 is the free term, β_i is the linear effect, β_{ii} is the squared effect, and β_{ij} is the interaction effect.

In this paper, the BFGS method, a branch of quasi-Newton methods, was used to solve function (7). This method is an effective method for solving nonlinear functions [25], and it has proven to be very successful through numerical experiments [26]. The RSM models of diameters and wall thicknesses were obtained with the help of the mathematical analysis software 1stOpt according to the parameters in Table 3. The RSM model of the diameter is recorded as $f_1(x)$, and it can be described by equation (8). The RSM model of the wall thicknesses is recorded as $f_2(x)$, and it can be described by equation (9).

Table 3: Orthogonal test schemes.

Test serial numbers	Factors			Corresponding parameters			Results	
	A	B	C	q (ml/min)	v (m/min)	n (r/min)	D (mm)	T (mm)
1	A_1	B_1	C_1	3	6	4	1.381	0.242
2	A_1	B_2	C_2	3	12	8	1.618	0.229
3	A_1	B_3	C_3	3	18	12	1.407	0.207
4	A_1	B_4	C_4	3	24	16	1.037	0.236
5	A_2	B_1	C_2	4	6	8	1.701	0.208
6	A_2	B_2	C_1	4	12	4	1.235	0.176
7	A_2	B_3	C_4	4	18	16	1.607	0.186
8	A_2	B_4	C_3	4	24	12	1.123	0.192
9	A_3	B_1	C_3	5	6	12	2.174	0.185
10	A_3	B_2	C_4	5	12	16	1.895	0.173
11	A_3	B_3	C_1	5	18	4	0.902	0.146
12	A_3	B_4	C_2	5	24	8	0.878	0.175
13	A_4	B_1	C_4	6	6	16	2.557	0.181
14	A_4	B_2	C_3	6	12	12	1.686	0.175
15	A_4	B_3	C_2	6	18	8	1.212	0.164
16	A_4	B_4	C_1	6	24	4	0.557	0.125

$$\begin{aligned} f_1(x) &= f_1(q,v,n) = 1.1072386318 \\ &\quad - 0.0475113618q + 0.0203636365v + 0.1066562500n \\ &\quad - 0.0053636364q \cdot v + 0.0125000000q \cdot n - 0.0038873106v \cdot n \\ &\quad - 0.0037500001q^2 - 0.0002673611v^2 - 0.0024531250n^2. \end{aligned} \tag{8}$$

$$\begin{aligned} f_2(x) &= f_2(q,v,n) = 0.4999772724 \\ &\quad -0.0933749999q - 0.0086969697v - 0.0035653409n \\ &\quad +0.0000151515q \cdot v + 0.0011988636q \cdot n + 0.0003456439v \cdot n \\ &\quad +0.0073750000q^2 + 0.0001527778v^2 - 0.0002734375n^2. \end{aligned} \tag{9}$$

4.2. Description Accuracy. To check the description accuracy of (8) and (9), the predicted diameters and wall thicknesses were predicted using RSM models under the same parameters, and the discrete points are shown in Figure 4. It can be seen from Figure 4 that the points are distributed near the curves, which indicates that the errors between the prediction results and the simulation results are smaller.

To further verify the effectiveness of the RSM models, the correlation coefficient R^2 was used as (10) [27]. The R^2 values of diameter and wall thickness are 0.987 and 0.973, respectively. The high R^2 (>0.95) values indicate that the developed models can truly reflect the relationship between the goals and extrusion process parameters.

$$R^2 = 1 - \frac{\sum (y_i - f_i)^2}{\sum (y_i - \overline{y})^2}, \tag{10}$$

where y_i is the value of experiment; f is the value of predicted; and $\overline{y}$ is the value of mean.

5. Multiobjective Optimization

5.1. Problem Description. In this paper, three different size characteristics (diameter D, wall thickness T) (1, 0.15), (1, 0.2), and (1.5, 0.2) were selected as the optimization goal. It can be known from Table 3 that the wall thickness in test 11 is 0.146 mm, which is close to the target size of 0.15 mm, but the error of the diameter compared with the target value of 1 mm is 9.8%; the wall thickness in test 8 is 0.192 mm, which is close to the target size of 0.2 mm, but the error of the diameter compared with the target value of 1 mm is 12.3%. It shows that there are conflicts between multiple targets, which means that optimizing only one objective may make another worse. A multiobjective optimization method should be used to find the optimization results of diameter and wall thickness to make all the objective functions reach the minimum value at the same time. The core of this method is to coordinate the relationship between objective functions and find the optimal solution set that makes each objective function relatively optimized as well as possible. If a problem has m targets to be optimized and each target has n optimization variables, the multiobjective optimization problem can be expressed as the following equation:

$$\min F(x) = \left[f_1(x), f_2(x), \cdots, f_m(x)\right]^T, \tag{11}$$

where the objective function $F(X)$ contains $m\,(m \geq 2)$ goals. The multiobjective optimization functions $F(X)$ should generally be as small as possible. Equation $F(X)$ is constructed based on the error between the predicted size and the target size of diameter and wall thickness in the paper to achieve the above requirements. According to the three

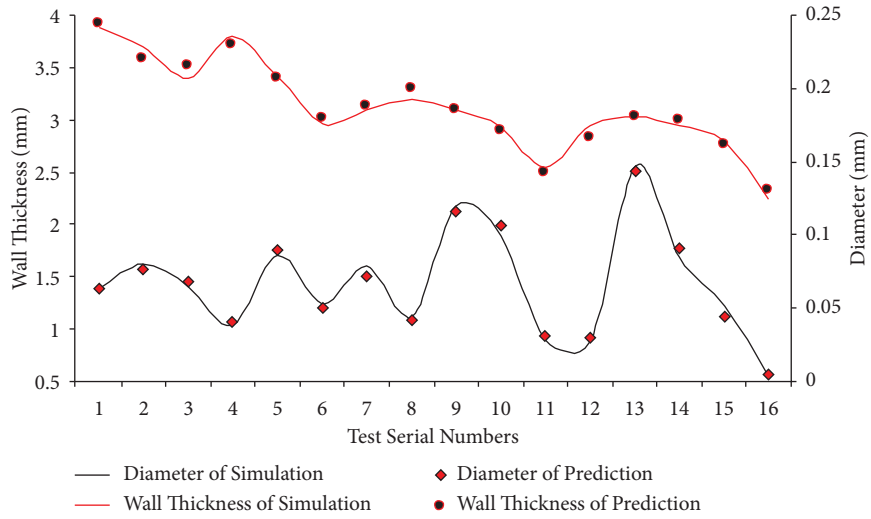

Figure 4: Diameter and wall thickness of simulation and prediction.

target sizes set above as well as the process parameters and their value ranges in Table 3, the extrusion process parameters optimization problem for the target size can be described as follows:

$$\min F(x) = \left[f_1(q, v, n) - D_0, f_2(q, v, n) - T_0 \right]^T, \quad (12)$$

where $q \in [3, 6]$, $v \in [6, 24]$, and $n \in [4, 16]$; $(D_0, T_0) = \{(1, 0.15), (1, 0.2), (1.5, 0.2)\}$.

5.2. Optimization Equation Solution through NSGA-II. In order to solve the multiobjective optimization problem (12), the multiobjective optimization algorithm (NSGA-II) is applied. This algorithm was proposed by Kalyanmoy Deb [28]. The key steps of the algorithm mainly include layering the NSGA-II algorithm, selecting operators according to the dominance relationship between individuals, using the fitness value allocation sharing strategy of noninferior solutions, and maintaining the diversity of each noninferior individual [29]. The flow chart of NSGA-II is shown in Figure 5.

5.3. Results and Discussion. In the process of solving with the NSGA-II algorithm, the population size is set to 50, the mutation probability is set to 0.25, the crossover probability is set to 0.8, and the maximum generation number is set to 2000. The Pareto coefficient is 1. Figure 6 shows the functional relations of optimal solutions with diameter f_1 and wall thickness f_2 of 50 solutions in the Pareto optimal solution set.

It can be seen from Figure 6 that the error of the optimization result is small, and the Pareto solution becomes more regular. The parameters for three sets of target sizes were optimized, and 5 optimization results of 15th, 20th, 25th, 30th, and 35th were selected from the 50 Pareto optimization results. The selection results and the corresponding diameter and wall thickness errors under this set of parameters are listed in Tables 4–6, respectively.

It can be seen from Tables 4–6 that the five sets of optimal process parameters obtained under each target size fluctuate in a small range, indicating that the optimization results are all convergent using NSGA-II. A set of parameter optimization solutions for the target size are obtained by averaging the optimization results of each group of 5 parameters and then rounding them. Table 7 shows three sets of optimization parameters for the above three target dimension characteristics of the microtubes, and the results of the diameters and wall thicknesses were solved through numerical simulation. It can be seen from Table 7 that the errors between the numerical simulation and the predicted value of three different target size characteristics (1, 0.15), (1, 0.2), and (1.5, 0.2) are less than 10%. The mean diameter error and wall thickness errors are 7.5% and 7.7%, respectively. The maximum error is 9.3%, and the minimum one is 5.3%.

6. Extrusion Experimental Verification

To verify the practicability and accuracy of the optimized system and its results, the optimized parameters obtained by NSGA-II in Table 7 are tested through experiments. The experimental material was polypropylene (PP, T30S, Dalian Petrochemical Corporation, China). The extrusion system consists of a single-crew extruder (HPE-100H, Davis-Standard Corporation, US) which has a diameter of 25 mm and a length-diameter ratio of 24 : 1. The structural dimensions of the die and the mandrel forming part are manufactured as in Table 1. The injection hole of the mandrel adopts a progressive step hole, and the diameter of the smallest part is 0.3 mm. The EDM (electric discharge machining) technology is adopted to manufacture the gas injection hole, and the assembly of the die is shown in Figure 7. Five samples were collected during each extrusion process. The average measurements were used as the experimental results. The profiles of the three microtubes are imaged as shown in Figure 8.

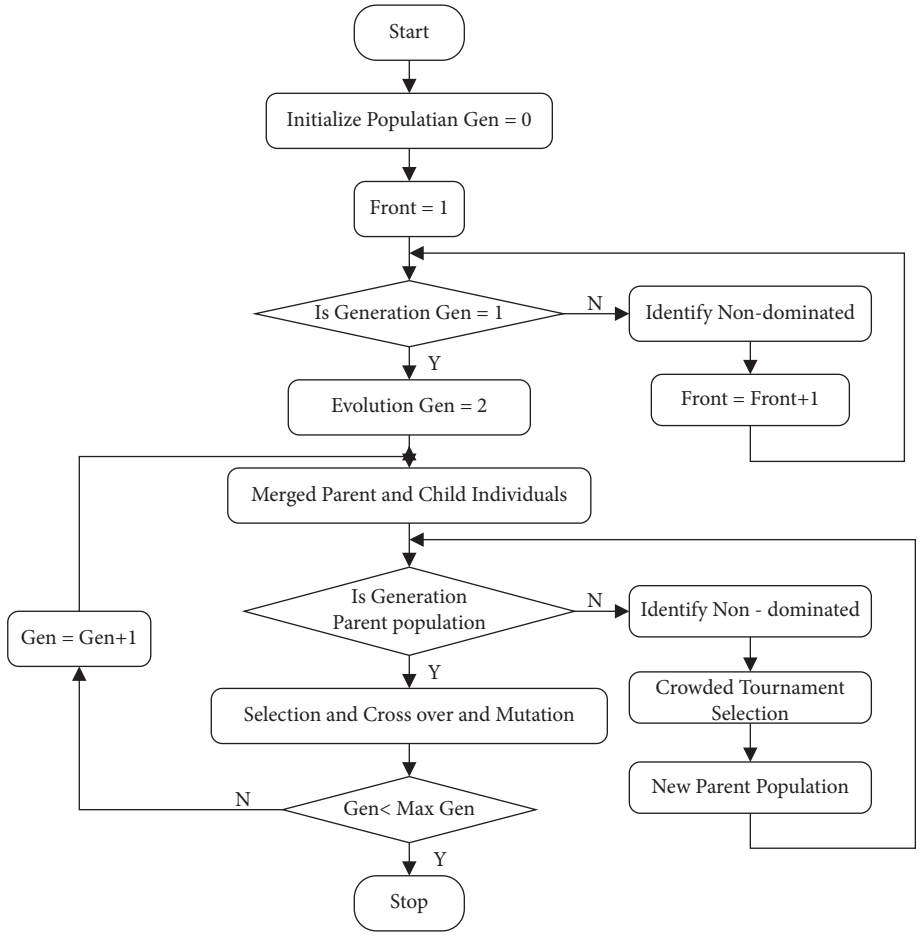

Figure 5: Flowchart of the NSGA-II.

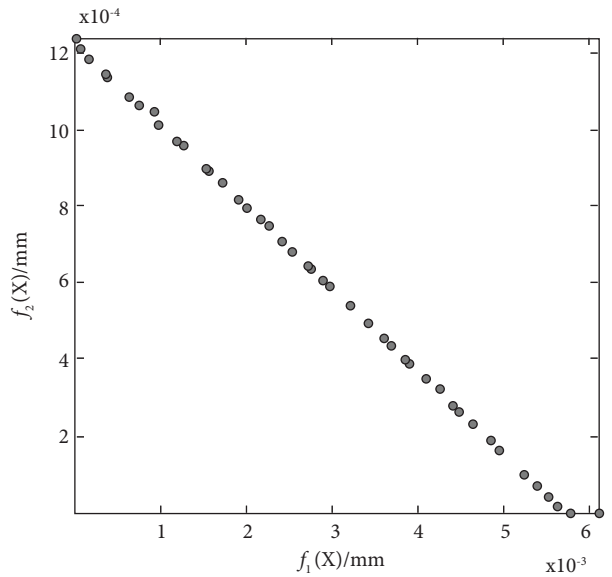

Figure 6: Optimal solutions for the diameter f_1 and wall thickness f_2.

The error between experimental results and target dimensions is compared with a reference range of 10% in Figure 9. It can be seen from Figure 9 that the diameter and wall thickness errors of the experimental are both less than 10%, which is an acceptable error range. In fact, the mean error is 6.53%, with the mean diameter error and wall

Table 4: Five optimal solutions of target size (1, 0.15).

Numbers	Process parameters			Results error	
	q (ml/min)	v (m/min)	n (r/min)	D (mm)	T (mm)
15	5.8452	18.0556	6.1905	$8.81e-5$	$6.58e-7$
20	5.8443	18.0554	6.1905	$1.07e-5$	$9.09e-7$
25	5.8452	18.0556	6.1905	$8.81e-5$	$6.58e-7$
30	5.8449	18.0556	6.1905	$6.10e-5$	$7.89e-7$
35	5.8569	18.0627	6.1905	0.0017	$7.87e-9$

Table 5: Five optimal solutions of target size (1, 0.2).

Numbers	Process parameters			Results error	
	q (ml/min)	v (m/min)	n (r/min)	D (mm)	T (mm)
15	5.9991	23.9978	13.7028	$7.38e-5$	0.0013
20	6	23.9978	13.7028	$1.18e-4$	0.0013
25	6	24	13.8333	0.0024	$7.05e-4$
30	6	24	13.9345	0.0045	$2.67e-4$
35	6	24	13.9660	0.0051	$1.31e-4$

Table 6: Five optimal solutions of target size (1.5, 02).

Numbers	Process parameters			Results error	
	q (ml/min)	v (m/min)	n (r/min)	D (mm)	T (mm)
15	3.7831	9.3354	5.7199	0.0561	$4.06e-8$
20	3.9479	8.0639	6.0319	$3.71e-5$	$4.79e-4$
25	3.9474	8.1750	6.0676	$1.55e-4$	$5.14e-5$
30	3.9912	7.8765	5.9756	0.0020	$2.49e-5$
35	3.7831	9.3354	5.7199	0.0561	$4.06e-8$

Table 7: Optimal solutions and simulation results.

$f(D, T)$	Optimal parameters			Simulation results		Error	
	q (ml/min)	v (m/min)	n (r/min)	D (mm)	T (mm)	D (%)	T (%)
(1, 0.15)	6	18	6	0.947	0.163	5.3	8.7
(1, 0.2)	6	24	14	1.093	0.189	9.3	5.5
(1.5, 0.2)	4	8	6	1.617	0.218	7.8	9

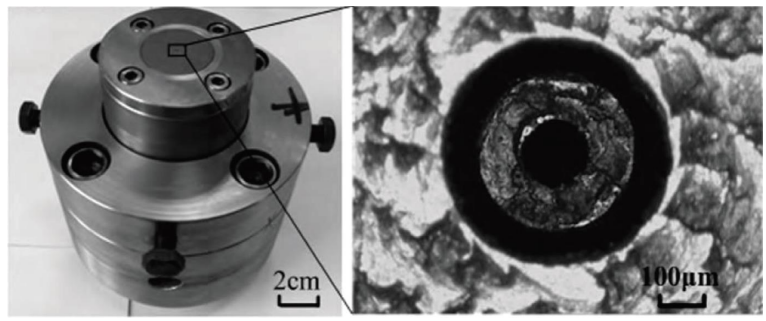

Figure 7: Single-lumen extrusion die and its cross-section.

thickness error of 7.3% and 5.77%, respectively. The maximum one is 9%, and the minimum one is only 1.3%. The results show that the diameter and wall thickness of the microtubes extruded based on optimizing the process parameters by using the optimization system have high accuracy relative to the target size, indicating that the system has certain practicability. All of these indicate that the extrusion process parameters optimal system designed by the numerical simulation based on the DCPP model and the hybrid method of RSM and NSGA-II is an effective method to quickly obtain the extrusion process parameter sets of the microtubes with target size features.

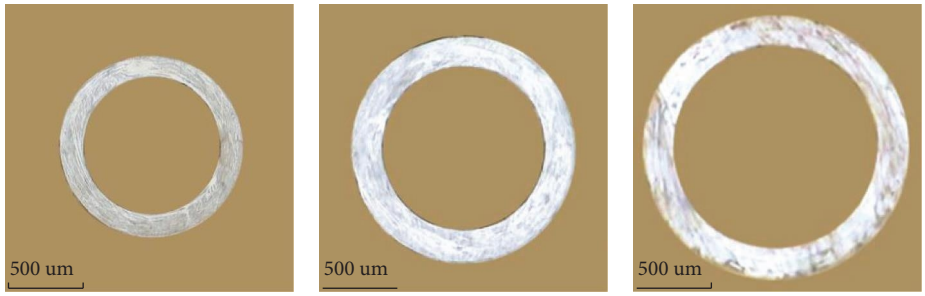

Figure 8: Cross-sections of the target microtubes: (a) (1.0, 0.15), (b) (1.0, 0.20), and (c) (1.5, 0.20).

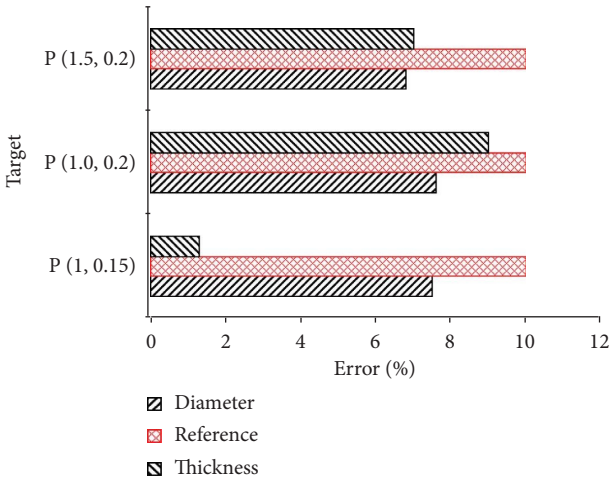

Figure 9: Error between experimental result and target dimensions compared with 10%.

7. Conclusions

The greatest contribution of this article is that the optimization system of extrusion process parameters was designed for rapidly extruding microtubes with a target diameter and wall thickness. Firstly, the double convected pom-pom (DCPP) model was selected for the numerical simulation of the tube extrusion process, and different process parameters and their corresponding simulation results were extracted based on orthogonal experiments. Secondly, the nonlinear functional relationships between microtube diameter and wall thickness with process parameters were established based on the response surface model (RSM). Finally, the nondominated sorting genetic algorithm II (NSGA-II) and response surface model (RSM) were mixed to find the optimal process parameters. Some experiments were carried out by taking three target tubes to evaluate the proposed system. The experimental results demonstrate that the average error of diameter and wall thickness of the three microtubes is 6.53%. The average diameter error and wall thickness error were 7.3% and 5.77%, respectively. The maximum value was 9%, and the minimum value was only 1.3%. These results indicate that the extrusion process parameter optimization system designed by the RSM-NSGA-II hybrid method based on the numerical simulation with the DCPP model is an effective and useful method to quickly obtain the extrusion process parameters of microtubes with target size features. Moreover, the system, which has the advantages of high efficiency, low cost, and high precision, is suitable for rapid extrusion of target microtubes in industrial production.

Data Availability

The processed data required to reproduce these findings cannot be shared at this time as the data also form part of an ongoing study.

Conflicts of Interest

The authors declare that they have no conflicts of interest.

Acknowledgments

This paper was supported by the Key Scientific Research Projects of the Chaohu University (grant no. XLZ-202103) and the Key Laboratory Project of the Chaohu University (grant no. kj20zsys03).

References

[1] W. C. Chang and D. W. Sretavan, "Microtechnology in medicine: the emergence of surgical micro devices, "Clin," *Neurosurgery*, vol. 54, pp. 137–147, 2007.

[2] D. Lalli, "Cycle-to-cycle Control of the Angioplasty Balloonfabrication Process," Master's Thesis, McGill University, Montreal, Canada, 2010.

[3] X. Z. Deng, S. F. Yu, and B. Xiao, "Research progress in polymer micro extrusion molding process," *"Rubber and Plastics Technology and Equipment*, vol. 43, no. 10, pp. 28–32, 2017.

[4] W. D. Zou, "Study on extrusion processing of profile pipe with small cross-section," M. Eng thesis. Dissertation, Beijing University of Chemical Technology, Beijing, China, 2006.

[5] W. Huang, "Research on gas-assisted molding equipment and process of double-lumen medical catheter," Master's thesis, Beijing University of Chemical Technology, Beijing, China, 2008.

[6] J. Henry, "A study of effects of select processing and material variables on jacket shrinkage in a PVDF-HFP tube-on extrusion process," Master's thesis, University of Massachusetts, Lowell, MA, USA, 2003.

[7] Y. W. Chen, "Research on PA11 micro tube precision extrusion molding process," Master's thesis, South China University of Technology, Guangzhou, China, 2011.
[8] X. Gong, "Numerical simulation of micro tube extruder head flow channel and micro tube forming research," Dissertation, South China University of Technology, Guangzhou, China, 2009.
[9] X. J. Fu, Y. Liu, and T. Lu, "The influence of machine head temperature on the forming dimensions of thin-walled small-diameter hoses," *Modern Plastics Processing and Applications*, vol. 13, no. 3, pp. 30–32, 2000.
[10] Y. F. Jin, "The Rheological Theories and Experimental Research on Polymer Micro Extrusion Process," Dissertation, Dalian University of Technology, Dalian, China, 2016.
[11] F. Wang, M. Sohail, U. Nazir, E. R. El-Zahar, C. Park, and N. Jabbar, "An implication of magnetic dipole in Carreau Yasuda liquid influenced by engine oil using ternary hybrid nanomaterial," *Nanotechnology Reviews*, vol. 11, no. 1, pp. 1620–1632, 2022.
[12] R. M. Khan, N. Imran, Z. Mehmood, and M. Sohail, "A Petrov–Galerkin finite element approach for the unsteady boundary layer upper-convected rotating Maxwell fluid flow and heat transfer analysis," *Waves in Random and Complex Media*, vol. 2022, Article ID 2055201, 18 pages, 2022.
[13] Y. Zhou, L. Luo, W. Liu, G. Zeng, and Y. Chen, "Preparation and characteristic of PC/PLA/TPU blends by reactive extrusion," *Advances in Materials Science and Engineering*, vol. 2015, Article ID 393582, 9 pages, 2015.
[14] G. H. Dai, Q. Q. Zhang, and G. B. Jin, "A model developed for predicting uniformity of kyphoplasty balloon wall thickness based on the orthogonal test," *Advances in Materials Science and Engineering*, vol. 2020, Article ID 1643080, 8 pages, 2020.
[15] N. Clemeur, R. P. Rutgers, and B. Debbaut, "On the evaluation of some differential formulations for the pom–pom constitutive model," *Rheologica Acta*, vol. 42, no. 3, pp. 217–231, 2003.
[16] H. Q. Tian, D. Y. Zhao, M. J. Wang, G. Jin, and Y. Jin, "Study on extrudate swell of polypropylene in double-lumen micro profile extrusion," *Journal of Materials Processing Technology*, vol. 225, pp. 357–368, 2015.
[17] A. Lawal and D. M. Kalyon, "Nonisothermal model of single-screw extrusion of generalized Newtonian fluids," *Numerical Heat Transfer, Part A: Applications*, vol. 26, no. 1, pp. 103–121, 1994.
[18] J. L. Zheng, D. W. Ge, and Y. W. Chen, "Variation of diameter and wall thickness of single-cavity medical micro tube extrusion molding," *Plastics*, vol. 41, no. 2, pp. 24–27, 2012.
[19] R. Guénette and M. Fortin, "A new mixed finite element method for computing viscoelastic flows," *Journal of Non-newtonian Fluid Mechanics*, vol. 60, no. 1, pp. 27–52, 1995.
[20] C. Y. Huang, H. H. Liu, and X. Y. Huang, "Numerical simulation of gas-assisted extrusion process of micro tube," *China Plastics Industry*, vol. 43, no. 10, pp. 44–47, 2015.
[21] G. B. Jin, "Research on design and manufacturing technology and extrusion process of polymer micro-extrusion dies for interventional medical catheters," Dissertation, Dalian University of Technology China, Dalian, China, 2013.
[22] G. Taguchi, "Performance analysis design," *International Journal of Production Research*, vol. 16, no. 6, pp. 521–530, 1978.
[23] U. Caydas and A. Hascalik, "A study on surface roughness in abrasive waterjet machining process using artificial neural networks and regression analysis method," *Journal of Materials Processing Technology*, vol. 202, no. 1-3, pp. 574–582, 2008.
[24] C. Lv, "The Optimization of Process Conditionals and Perform Structural Parameters for PET Bottles," Dissertation, Zhejiang University, Hangzhou, China, 2014.
[25] D. H. Li and M. Fukushima, "A globally and super linearly convergent Gauss-Newton-based BFGS method for symmetric nonlinear equations," *SIAM Journal on Numerical Analysis*, vol. 37, no. 1, pp. 152–172, 1999.
[26] Z. Wei, G. Li, and L. Qi, "New quasi-Newton methods for unconstrained optimization problems," *Applied Mathematics and Computation*, vol. 175, no. 2, pp. 1156–1188, 2006.
[27] P. S. Ghosal and A. K. Gupta, "Enhanced efficiency of ANN using non-linear regression for modeling adsorptive removal of fluoride by calcined Ca-Al-(NO3)-LDH," *Journal of Molecular Liquids*, vol. 222, pp. 564–570, 2016.
[28] K. Deb, A. Pratap, S. Agarwal, and T. Meyarivan, "A fast and elitist multi objective genetic algorithm: nsga- II," *IEEE Transactions on Evolutionary Computation*, vol. 6, no. 2, pp. 182–197, 2002.
[29] Y. Rong, Q. Zhou, Y. Huang, Y. Chang, G. Zhang, and X. Shao, "Multi-objective optimization of laser brazing with the crimping joint using ANN and NSGA-II," *International Journal of Advanced Manufacturing Technology*, vol. 85, no. 5-8, pp. 1239–1247, 2016.